# Radar Observation of Evaporation and Implications for Quantitative Precipitation and Cooling Rate Estimation

XINXIN XIE, RAQUEL EVARISTO, SILKE TROEMEL, PABLO SAAVEDRA, AND CLEMENS SIMMER

*Meteorological Institute, University of Bonn, Bonn, Germany*

ALEXANDER RYZHKOV

*Cooperative Institute for Mesoscale Meteorological Studies, University of Oklahoma, and NOAA/OAR/National Severe Storms Laboratory, Norman, Oklahoma*

(Manuscript received 7 December 2015, in final form 15 June 2016)

ABSTRACT

This study analyzes radar observations of evaporation in rain and investigates its impact on surface rainfall and atmospheric cooling rates. A 1D model is used to examine the impact of raindrop evaporation on the evolution of the initial raindrop size distribution (DSD), the resulting reflectivity ($Z$), and differential reflectivity ($Z_{DR}$) and surface rain rates. Raindrop evaporation leads to a decrease of $Z$ and an increase of $Z_{DR}$ toward the surface because of the depletion of small raindrops that evaporate first and thus enhance the mean raindrop size. The latter effect, however, can be reduced because of the increasing temperature toward the surface and may even lead to a decrease of $Z_{DR}$ toward the surface. Two events with significant rain evaporation, observed simultaneously by a polarimetric X-band radar and a K-band Micro Rain Radar (MRR), offer quite detailed insight into the evaporation process. During the first event, which exhibits an initial $Z_{DR} > 1.5$ dB in the upper rain column, raindrops undergo relatively weak evaporation as deduced from the decrease of the small raindrop fraction observed by the MRR. The second event is characterized by a lower initial $Z_{DR} < 0.5$ dB with all raindrops evaporating before reaching the ground. A retrieval scheme for estimating the evaporation-related cooling rate and surface precipitation from polarimetric radar observations below the bright band is derived based on MRR observations. The algorithm is then used to simulate polarimetric X-band radar observations, which might mitigate uncertainties in the surface rainfall retrievals due to evaporation at far distances from the radars and in the case of beam blocking.

## 1. Introduction

Precipitation processes depend on ambient environmental conditions, which lead to different evolutions of the initial drop size distributions (DSD) (Pruppacher and Klett 1997). When raindrops fall through unsaturated air, their initial DSD evolves subject to a variety of microphysical processes. While collisional processes (coalescence and breakup) and size sorting do not deplete the overall amount of liquid water (Prat and Barros 2007; Kumjian and Prat 2014), evaporation preferably depletes the small raindrops and might lead to significant reductions of surface precipitation compared to its values aloft (Gori and Joss 1980; Hu and Srivastava 1995). Evaporative cooling may produce or increase downdrafts below the cloud base and thus influence the strength of cold pools and the initiation and lifetime of new convective systems (Srivastava 1987; Seifert 2008). Therefore, the quantification of rain evaporation is important not only for surface rainfall estimation from radar observations but also for a better understanding of convective initiation and storm dynamics.

Radar observations have been already used to estimate evaporation effects on derived rain rates, for example, by Rosenfeld and Mintz (1988). Substantial evaporation of drizzle below marine boundary layer clouds has been quantified using ship-based radar measurements, and significant uncertainties in the surface rainfall retrievals result from neglecting such effects (Comstock et al. 2004). Since evaporation is drop size

*Corresponding author address*: Xinxin Xie, Meteorological Institute, University of Bonn, Auf dem Huegel 20, 53121 Bonn, Germany.
E-mail: xxie@uni-bonn.de

DOI: 10.1175/JTECH-D-15-0244.1

sensitive, it impacts the DSD evolution and thus also the relationship between radar reflectivity $Z$ and rain rate. Neglecting evaporation effects on DSDs may lead to an overestimation of surface rain rates (Li and Srivastava 2001).

Polarimetric radars help to reduce the uncertainties in quantitative precipitation estimation (QPE) caused by nonrain hydrometeors and DSD variability, and even allow for DSD retrievals (Zhang et al. 2001; Brandes et al. 2004; Gorgucci et al. 2008; Kim et al. 2010). For example, Li and Srivastava (2001) proposed a reflectivity–differential reflectivity–rain rate ($Z$–$Z_{DR}$–$R$) relationship for more robust rainfall retrievals; such methods do not, however, account for the DSD evolution from the lowest radar-observed height to the surface. Kumjian and Ryzhkov (2010) simulated the sensitivity of polarimetric variables to evaporation at S and C bands and evaluated different DSD retrieval algorithms with a 1D model, in order to better understand the polarimetric fingerprint produced by the evaporation process. Raindrop evaporation changes the DSD and reduces the rainwater mass. Borowska et al. (2011) concluded from one-month polarimetric radar observations that the observed increase in $Z_{DR}$ toward the surface must be attributed to evaporation. Penide et al. (2013) investigated two wet season events observed by a C-band polarimetric radar and interpreted the increase of the retrieved mean volume diameter toward the surface as the signature of evaporation below the cloud base in drier environments. A 15-yr statistical analysis of spaceborne precipitation radar observations revealed that evaporation in dry environments is likely to reduce rain rate toward the surface, especially in light precipitation (Cao and Qi 2014).

Though many studies exist on rainfall evaporation observed by precipitation radars, no comprehensive study exists, which corroborates such observations with DSD observations and/or quantitative microphysics-based simulations. The motivation of this study, which relates observations of a vertically pointing K-band Micro Rain Radar (MRR) and a polarimetric X-band radar in Bonn, Germany (BoXPol), to DSD evolutions, is to contribute to the improvement of QPE from radar polarimetry, to a better understanding of DSD evolution, and to the estimation of cooling rates caused by evaporation.

The paper is organized as follows. Section 2 introduces a simple 1D evaporation model together with an analysis of the sensitivity of polarimetric variables and surface precipitation to initial DSDs below the bottom of the melting layer. Observations of evaporation by the polarimetric X-band radar and a collocated vertically pointing K-band MRR deployed in Bonn, Germany, are presented in section 3, to corroborate the sensitivity study presented in section 2. While the X-band polarimetric radar observes microphysical fingerprints produced by the evaporation process, the MRR provides an efficient tool for a more direct view into the DSD evolution. Based on these observations, section 4 suggests a method that uses $Z$ and $Z_{DR}$ aloft for surface rainfall estimation taking account evaporation. Such a methodology might be useful for QPE when only radar observations at higher elevations are available due to complex terrain or large distances away from the radar. The impact of evaporation on evaporative cooling rates will be examined using radar observations in section 5. Finally, conclusions and an outlook are given in section 6.

## 2. Evaporation model

In this section, a simple evaporation model that neglects vertical air motion is derived, in order to investigate the impact of evaporation on DSD evolution, subsequent X-band polarimetric observables, and surface rain rates. In subsaturated conditions, raindrops evaporate by the diffusion of water vapor from the raindrop surface into the ambient air. The rate of mass diffusion for this process, given by Rogers and Yau (1989), Li and Srivastava (2001), and Kumjian and Ryzhkov (2010), is expressed by

$$\frac{dm}{dt} = 2\pi D D_v f_v \Delta\rho_v, \tag{1}$$

where $m$ is the mass of the raindrop with diameter $D$; and $D_v$ and $f_v$ are the diffusion and ventilation coefficients of water vapor in air, respectively; and $\Delta\rho_v$ is the difference of vapor density between the environment and the raindrop surface.

Following Rogers and Yau (1989) and Pruppacher and Klett (1997), the rate of change of $D$ can be approximated as

$$D\frac{dD}{dt} = 4\frac{S-1}{F_K + F_D}, \tag{2}$$

where $S$ is the ambient air saturation ratio and $F_K$ and $F_D$, following the derivations of Rasmussen and Heymsfield (1987), Rogers and Yau (1989), and Kumjian and Ryzhkov (2010), are terms associated with heat conduction and vapor diffusion, respectively.

In the model, we assume raindrops with diameters ranging from 0.05 to 8 mm, which evolve solely subject to evaporation. The raindrops are assumed to attain terminal velocity $v_t$ according to Brandes et al. (2002):

$$v_t(D) = -0.1021 + 4.932D - 0.9551D^2 + 0.079\,34D^3 - 0.002\,362D^4, \quad (3)$$

with $D$ in millimeters and $v_t$ in meters per second . Thus, Eq. (2) can be rewritten as

$$v_t(D)D\frac{dD}{dH} = 4\frac{S-1}{F_K + F_D}, \quad (4)$$

where $H$ is the vertical distance below the initial height, which is assumed to be below the melting layer. Therefore, given its initial size, the corresponding raindrop diameter at each altitude can be derived accordingly by Eq. (4).

We now assume a 1D vertical rain shaft extending downward from the bottom of the melting level with the initial DSD following a normalized gamma distribution (Willis 1984; Testud et al. 2001),

$$N(D) = N'_w\left(\frac{D}{D_0}\right)^{\mu}\exp\left[-\frac{(3.67+\mu)D}{D_0}\right], \quad (5)$$

where $N'_w$ is the normalized concentration, $\mu$ is the shape parameter, and $D_0$ is the mean volume diameter. The variability of the initial DSD is modeled by varying the mean volume diameter $D_0$ between 0.25 and 2.5 mm, and the shape parameter $\mu$ between $-2$ and 12 following Anagnostou et al. (2008), while $N'_w$ is always adjusted to result in a constant initial rain rate of 5 mm h$^{-1}$. Other microphysical processes like coalescence, which might be important compared to evaporation in rain events with higher rain rates, are ignored. The raindrop temperature is assumed to be equal to the ambient temperature, since only subtle differences in the decrease of raindrop size during evaporation are introduced when comparing our simulations with the ones from Kumjian and Ryzhkov (2010). Raindrops are treated as horizontally oriented oblate spheroids with aspect ratios (ARs) depending on raindrop diameter (mm) (Brandes et al. 2002):

$$\mathrm{AR} = 0.9951 + 0.025\,10D - 0.036\,44D^2 + 0.005\,303D^3 - 0.000\,249\,2D^4. \quad (6)$$

To investigate the sensitivity of polarimetric X-band moments to DSDs during rainfall subject to evaporation, we follow the atmospheric scenario used by Li and Srivastava (2001) and Kumjian and Ryzhkov (2010): the bottom of the melting layer is located at an altitude of 3000 m and a constant lapse rate of 10°C km$^{-1}$ is assumed. Thus, the ground surface temperature is 30°C. Relative humidity is fixed at 100% at the initial height level and decreases linearly toward the ground, while the surface relative humidity may vary between 0% and 100%. The polarimetric variables at X band are calculated by applying the T-matrix method (Mishchenko 2000) to the output of the described evaporation model.

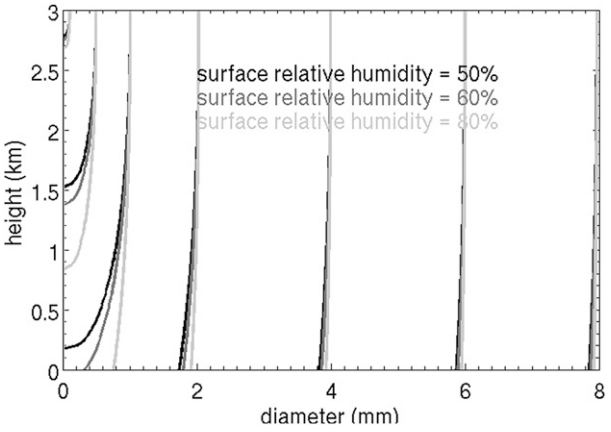


FIG. 1. Change of raindrop diameter with height for initial raindrop diameters of (left to right) 0.1, 0.5, 1, 2, 4, 6, and 8 mm. Relative humidity starts at 100% at 3 km and linearly decreases to 50%, 60%, and 80% at the surface, while temperature linearly increases below the bottom of melting layer toward the ground with a constant lapse rate of 10°C km$^{-1}$.

According to Eq. (4) raindrop diameters decrease in a subsaturated environment with $S < 1$, and the rate of the raindrop diameter change is inversely proportional to its diameter following Eq. (2). Figure 1 displays the simulated change of raindrop diameter as a function of height and demonstrates that smaller raindrops evaporate much faster than larger raindrops. In dry conditions, raindrops with an initial diameter $< 1$ mm may totally evaporate before reaching the surface, while for those with initial diameters $> 4$ mm, evaporation only marginally impacts their evolution. Drier atmospheres intensify evaporation, for example, raindrops with initial diameters of 0.5 mm evaporate totally already at an altitude above 1500 m when the surface relative humidity is 50%, whereas they survive down to an altitude of 850 m for a surface relative humidity of 80%.

Figure 2 shows $Z$ and $Z_{\mathrm{DR}}$ at X band as a function of the initial DSD below the bottom of the melting layer and compares $Z$ and $Z_{\mathrm{DR}}$ to their values at the surface. The simulations displayed in Fig. 2 assume that relative humidity linearly decreases to 50% at the ground. The terms $Z$ and $Z_{\mathrm{DR}}$ at 3000 m are illustrated by gray contour lines depending on the parameters of the initial DSDs for an initial rain rate of 5 mm h$^{-1}$. Larger $D_0$ leads to stronger backscattering (larger $Z$) and polarization (larger $Z_{\mathrm{DR}}$), resulting in $Z$ and $Z_{\mathrm{DR}}$ reaching up to 40 dB$Z$ and 2.5 dB, respectively. A larger shape parameter $\mu$ reduces the contribution of very large raindrops and thus leads to lower $Z$ and $Z_{\mathrm{DR}}$.

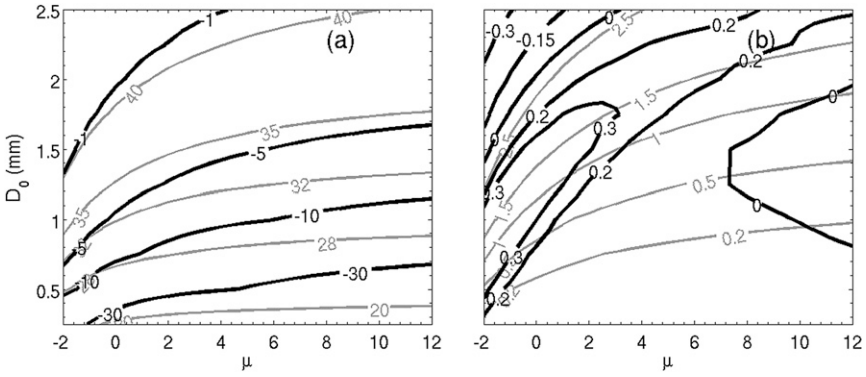


FIG. 2. Reflectivity ($Z$) and differential reflectivity ($Z_{DR}$ below the melting layer and their change toward the surface as a function of the initial DSDs. (a) The gray contour lines show the initial $Z$ at 3000 m as a function of mean diameter $D_0$ and shape parameter $\mu$ with 5 mm h$^{-1}$ rainfall intensity at that height. The black contour lines indicate the decrease of $Z$ due to evaporation at the ground level, i.e., $Z_{ground} - Z_{3000m}$, assuming the relative humidity decreases linearly from 100% at 3000 m to 50% at the surface. A surface temperature of 30°C is assumed with a lapse rate of 10°C km$^{-1}$. (b) As in (a), but for $Z_{DR}$, which mostly increases toward the surface, except for high $D_0$ and low or negative $\mu$.

Evaporation reduces the total mass of rainwater, while the mean raindrop size gradually increases compared to the initial DSDs aloft due to the preferential depletion of small raindrops. Thus, $Z$ decreases slowly toward the ground when predominantly the small raindrops evaporate (Fig. 2a). For example, for an initial $D_0$ below 0.5 mm leading to $Z < 28$ dB$Z$, the depletion of small raindrops leads to a decrease of $Z$ at the surface of up to 30 dB$Z$. With increasing initial $D_0$, the $Z$ reduction toward the surface by evaporation is lower, since larger raindrops evaporate much more slowly, for example, the $Z$ reduction is <5 dB$Z$ for $D_0 > 1$ mm. The increase of $D_0$ due to evaporation mostly enhances $Z_{DR}$ toward the ground with a maximum increase in the range of 0.3 dB (Fig. 2b). However, for an initial $D_0 > 1.5$ mm and $\mu < 2$, $Z_{DR}$ decreases toward the ground. Here the change of the dielectric with the increasing temperature toward the surface dominates the change of the scattering properties of the raindrops.

In the case of drizzle when small raindrops dominate the DSDs, the surface rain rate can approach zero (Fig. 3). Even for extreme DSDs with $D_0$ up to 2.5 mm, the rain rate can still be reduced by 30% when the near-surface relative humidity decreases to 50%, while the temperature increases to 30°C. The evaporative reduction of the rain rate is mainly a function of $D_0$ aloft and only to a lesser degree of $\mu$. An increase of $D_0$ in the initial rain shaft from 0.5 to 1.5 mm increases the surface rain rate from 0.5 to 2.5 mm h$^{-1}$ under the conditions mentioned above: the drier the atmosphere, the stronger the reduction of the rain rate at the surface (not shown). The model simulations are consistent with previous studies (Li and Srivastava 2001; Kumjian and Ryzhkov 2010).

## 3. Observations

In this section, two events are presented, based on observations from a polarimetric X-band radar and a K-band MRR, in order to corroborate the model results presented above. A short description of the instruments is followed by the analysis of the observations.

The BoXPol is deployed at an altitude of 99.9 m MSL on the roof of a building next to the Meteorological Institute at the University of Bonn, Germany. A detailed technical description of BoXPol can be found in Diederich et al. (2015). The bias of $Z$ observed by BoXPol is calibrated according to Diederich et al.

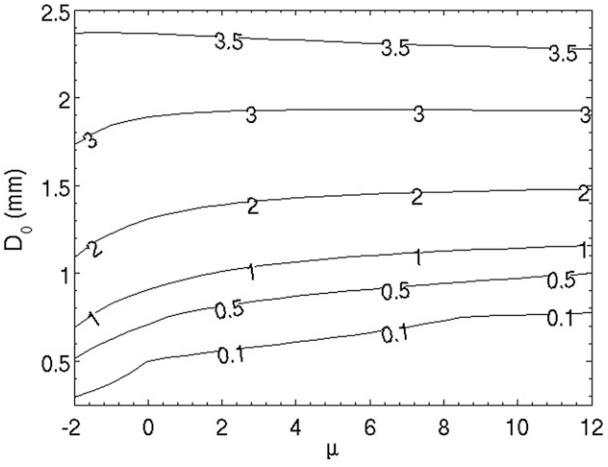


FIG. 3. The surface rain rate modified by evaporation as a function of the initial DSDs at 3000 m with an initial RR of 5 mm h$^{-1}$, assuming the relative humidity linearly decreases from 100% at 0°C to 50% and the temperature linearly increasing to 30°C at the surface.

(2015), and $Z_{DR}$ is bias corrected with the zenith scan. The MRR is deployed at a distance of ~200 m away from BoXPol. The MRR is a compact 24-GHz frequency-modulated continuous wave (FMCW) radar designed for the estimation of DSD profiles based on the detected Doppler spectra observed with a single-polarization receiver (for details, see Kneifel et al. 2011; Saavedra et al. 2012). The built-in signal processing of the MRR allows for clear identification of the ice phase, since the precipitation rate is drastically overestimated when assuming the same fall velocity for snow. The MRR detects raindrop sizes between 0 and 6 mm and operated during the two events with a vertical resolution of 150 m and 30 range gates. Since the closer range gates are affected by near-field scattering, only data above 600 m AGL are used in this study.

Figure 4 shows the prevalent temperature and relative humidity profiles on 4 July 2014. Two precipitation events are examined in detail later in this section, one beginning at 1450 UTC and the other at 2200 UTC. The relative humidity decreases toward the ground according to the radiosondes launched in Essen, Germany, which is about 90 km to the north of Bonn. At 1200 UTC the relative humidity near the surface was below 40% and increased to ~60% at 2400 UTC, indicating rather dry atmospheric conditions. The melting level varied in height between 3000 and 3500 m, while the surface temperature ranged between 20° and 30°C and decreased with altitude with a gradient of ~8°C km$^{-1}$. Ground-based observations by the meteorological station of the Meteorological Institute at the University of Bonn showed the 2-m temperature was 28.5°C at 1200 UTC and gradually decreased to 21°C at 2400 UTC, with a minor peak reaching 30.5°C at 1330 UTC. The relative humidity gradually increased from ~30% at 1200 UTC to 65% at 2400 UTC, which is consistent with the radiosonde observations. This dry atmosphere accompanied by warm temperatures offers quite favorable atmospheric conditions for the observations of evaporation during rainfall.

We first focus our analysis on the radar observations between 1450 and 1530 UTC, when the first precipitation event approached BoXPol from the southwest (azimuth direction of ~225°). A genuine RHI scan of BoXPol was performed at the same azimuth angle at 1450 UTC on this day (Fig. 5). Plan position indicators (PPI) at different elevations ranging from 1.5° to 14° indicate that the precipitating system was moving practically parallel to the RHI plane at all heights, thus significant advection into or out of the RHI scan can be excluded (not shown). The melting layer is clearly visible in terms of enhanced $Z$ and $Z_{DR}$ at ~3000-m altitude. Reflectivity close to the radar is >30 dB$Z$ and $Z_{DR}$ is >1.5 dB. At a horizontal distance of 4000 m away from BoXPol, both $Z$ and $Z_{DR}$ are smaller than when close to BoXPol. Previous studies have already shown that $Z_{DR}$ is mainly determined by the $D_0$ in DSDs (Bringi and Chandrasekar 2001; Kim et al. 2010). Thus, for the precipitation cell with the larger $Z_{DR}$ close to the radar, $D_0$ should be much larger than for the precipitating cells farther away that are seen in the RHI. Thus, the precipitating cells with larger raindrops come first and are followed by precipitating cells with smaller raindrops. Note that the $Z_{DR}$ at larger elevations close to BoXPol is estimated using the elevation dependency of $Z_{DR}$ (Ryzhkov et al. 2005), in order to compensate for the diminishing polarization of horizontally oriented spheroids with increasing elevations.

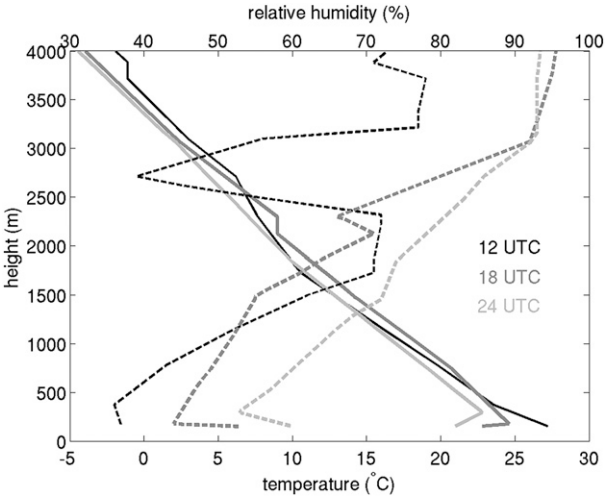


FIG. 4. Profiles of temperature (solid lines) and relative humidity (dashed lines) measured by the radiosondes launched in Essen, at 1200, 1800, and 2400 UTC 4 Jul 2014. Note that the height is above MSL.

Because of the dry atmospheric conditions, all raindrops are expected to undergo significant evaporation during their fall toward the ground. While the raindrop number concentration should be reduced predominantly for particles with small diameters, the mean diameter of DSDs should increase. This is consistent with the radar observations, since $Z$ at the surface is always lower than its value aloft below the bottom of the melting layer. Following the rain shaft (black solid lines in Fig. 5) at a horizontal distance of 1000–5000 m from BoXPol, $Z$ decreases from ~32 dB$Z$ below the melting layer to ~25 dB$Z$ near the ground; in another rain shaft at 6000–9000 m away from the radar, $Z$ decreases from ~25 to ~15 dB$Z$. At a distance of 4000 m, where $Z_{DR}$ is less affected by the oblique radar-viewing geometry, $Z_{DR}$ along the rain shaft increases slightly toward the ground, most probably due to the evaporation process, and in line with the sensitivity study presented in section 2.

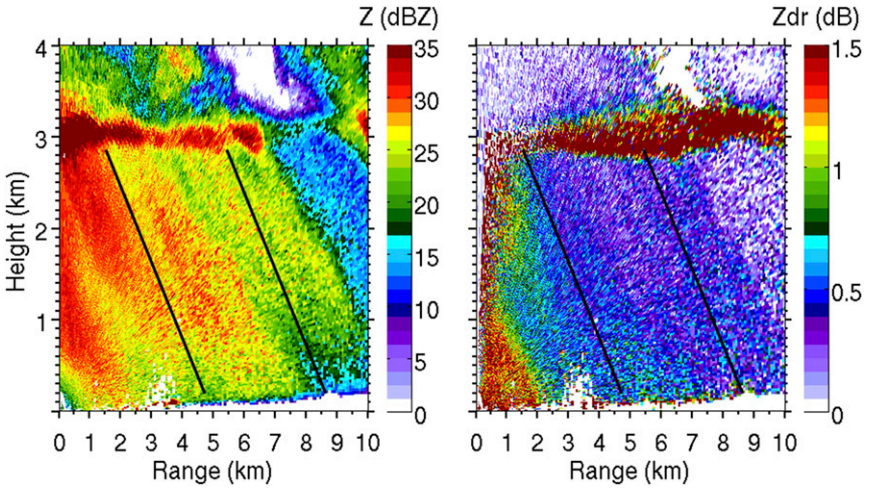


FIG. 5. The terms (left) $Z$ and (right) $Z_{DR}$ observed by a BoXPol RHI scan at an azimuth angle of 225° at 1450 UTC 4 Jul 2014. The solid black lines follow the rain shaft, which is tilted with respect to vertical.

The polarimetric fingerprint for evaporation is not always easily detected in polarimetric radar observations, and in some scenarios it is likely that the subtle changes in $Z$ and $Z_{DR}$ on the order of 1 dB$Z$ and 0.1 dB, respectively, are within the observational error. Especially when the initial mean volume diameter is large and the resulting reflectivity is above 40 dB$Z$, the identification of evaporation only from polarimetric radar observations becomes difficult (Fig. 2). Thus, observations from a collocated MRR provide useful additional information with its ability to resolve vertical DSD profiles.

Figure 6 shows the first precipitation event occurring between 1450 and 1530 UTC, as captured by the MRR. Between 1450 and 1500 UTC, precipitation is indicated via reflectivities reaching up to 30 dB$Z$. Although $Z$ does not vary much between 1450 and 1500 UTC, the DSD-derived rain rate (RR) decreases toward the surface from 2 to 1.5 mm $h^{-1}$ (Fig. 6b), presumably caused by evaporation. For the precipitating cells passing the MRR after 1500 UTC, both $Z$- and DSD-derived rain rates decrease toward the ground, also suggesting the evaporation process in action (Figs. 6a and 6b). Further evidence of evaporation can be drawn from the DSD evolution with height (Figs. 6c–f show the DSDs observed by the MRR at altitudes of 2700, 1950, 1200, and 600 m, respectively). At ~1455 UTC we observe that the maximum diameter of raindrops decreases from 6 to 5 mm toward 1950 m, which is probably caused by breakup. From 1950 m toward the ground, the number concentration of 5-mm raindrops barely changes, which implies that breakup is not the dominant process below 1950 m. The concentration of small raindrops decreases almost by an order of magnitude toward the ground, which confirms evaporation is prevail for this event, especially below 1950 m. Between 1450 and 1500 UTC, the number concentration of raindrops $< 1$ mm first increases from an altitude of 2700 to 1950 m presumably by the shrinking of larger drops, and then decreases gradually toward the ground (Fig. 6). Between 1505 and 1520 UTC, when rain rates gradually decrease toward the ground, the maximum diameter of raindrops decreases from 4 mm at 2700 m to 3 mm below 2700 m. In parallel, the concentration of small raindrops increases from 2700 to 1200 m followed by a reduction until complete extinction, again presumably by the shrinking of larger raindrops. The change in small raindrop concentration toward the ground must be caused by evaporation, since the rain rates recede toward the ground (Fig. 6b); collisional breakup, which can also induce an increase in small raindrop concentration, would not change the rain rates (Kumjian and Prat 2014) and cannot be responsible for the observed increase in small raindrop concentration. Therefore, evaporation is the dominant microphysical process that decreases rain rates and increases small raindrop concentration toward the ground.

A second event occurs between 2200 and 2230 UTC on the same day (4 July 2014). All passing precipitating cells reveal $Z < 30$ dB$Z$ and $Z_{DR} < 0.5$ dB according to the BoXPol RHI scan at azimuth angle 225° (Fig. 7). The BoXPol PPI scans at different elevations do not detect precipitating cells close to the radar and no precipitation falls out of the RHI plane (not shown). Both BoXPol and the MRR reveal that no precipitation reaches the ground.

The DSD evolution observed by the MRR reveals that the maximum raindrop diameters are all <3 mm with highest concentration at diameters around 1 mm at an

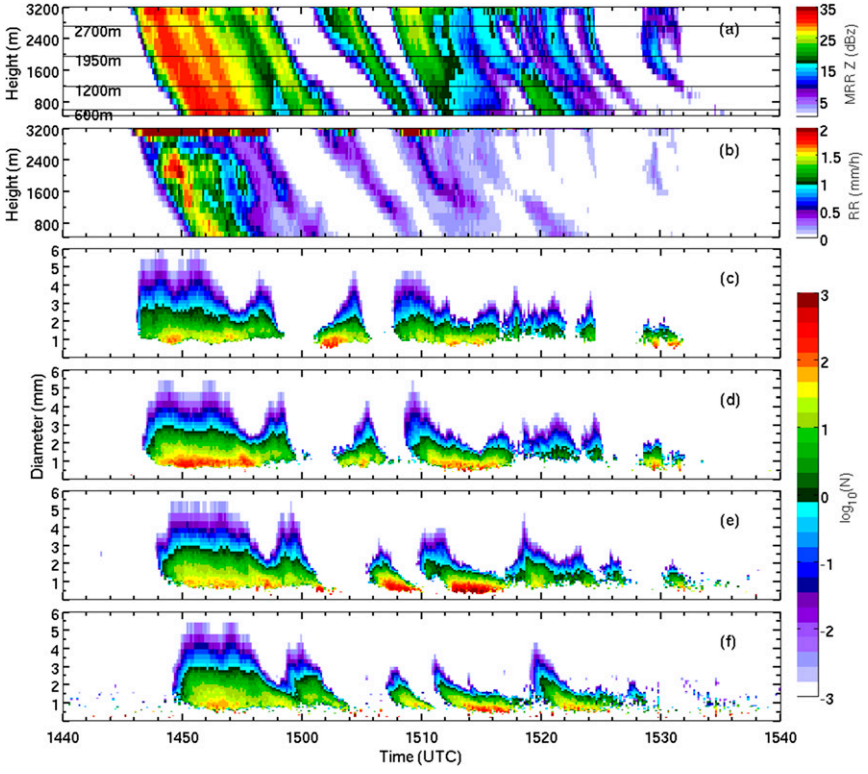


FIG. 6. MRR observations on 4 Jul 2014. (a) MRR-observed $Z$ with the black solid lines indicating the four altitudes, for which the DSD evolution is shown in (c)–(f). (b) MRR-observed RR. (c)–(f) Raindrop number concentration in logarithmic scale at altitudes of 2700, 1950, 1200, and 600 m, respectively.

altitude of 2700 m (Fig. 8). The fast evaporation process is highlighted by the depletion of raindrops: raindrops completely evaporate already at an altitude of ~1000 m. From the altitude of 2700 m down to the surface, the maximum diameter of raindrops diminishes gradually and the number concentration of small raindrops decreases toward the ground (e.g., at 2200–2210 UTC), which again suggests evaporation acting for this event.

## 4. Implications for rainfall estimation

From the observations we can infer that surface rain rates retrieved from observations at higher altitudes above the ground can be substantially overestimated when evaporation is not taken into account. To further examine the relation between evaporation-affected DSDs, the resulting surface rain-rate reductions, and changes in the polarimetric moments, T-matrix calculations for X band are performed using the vertical DSD profiles observed by the MRR (Figs. 6 and 8). The temperature profiles are interpolated from the radiosonde observations at 1200 and 2400 UTC at the observation station Essen.

Figures 9 and 10 show for both events "pseudo-observations" of BoXPol from the MRR-observed DSDs, together with the MRR observations. The similar patterns between simulated X-band and MRR reflectivities indicate the robustness of DSD estimated from the MRR observations despite small differences. Between 1450 and 1530 UTC (the first case), the simulated $Z$ at X band approaches 35 dB$Z$, while $Z_{DR}$ below the melting layer reaches up to 2 dB at the beginning of the observation, which is consistent with the BoXPol RHI scan at 1450 UTC (Fig. 5); otherwise, $Z_{DR}$ is <1 dB (Fig. 9). Note that the large $Z_{DR}$ near 1510 UTC at ~2000 m might be caused by size sorting (bigger raindrops falling faster than smaller drops). For the second event, the "pseudo-observed" $Z_{DR}$ below 0.5 dB is related to the predominantly small raindrops between 2200 and 2230 UTC on this day (Fig. 10). Unfortunately, a direct comparison of the observed BoXPol polarimetric variables moments and these pseudo-observations cannot be made due to the coarse temporal resolution of the BoXPol RHIs (every 5 min).

In subsaturated conditions the rain rate is reduced by evaporation when falling toward the surface and

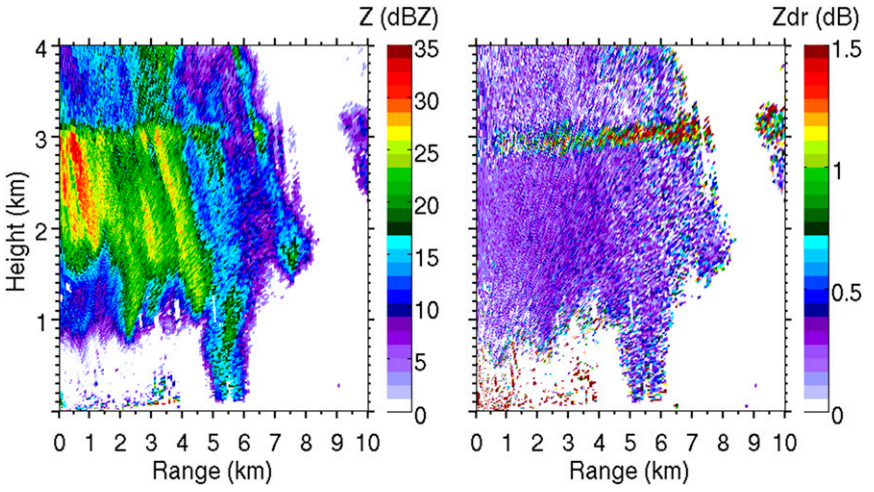


FIG. 7. As in Fig. 5, but for 2200 UTC 4 Jul 2014.

the assumption of a constant rain rate toward the ground is no longer applicable. The accuracy of surface rain-rate estimates may deteriorate, due to the increasing radar beam height with an increasing distance to the radar. Especially in mountainous regions where the complex topography restricts radar observations, only polarimetric observables aloft are available for the retrievals of the surface rain rate, which might lead to similar errors even at closer distances to the radar.

Both the surface rain-rate reduction due to evaporation and the $Z_{DR}$ aloft highly depend on the DSD aloft (mainly on $D_0$). This connection can be exploited to improve retrieval algorithms of rain rates at the surface. Cross-checking the MRR-observed rain-rate reduction in the rain column (Figs. 6 and 8) and the pseudo-observed

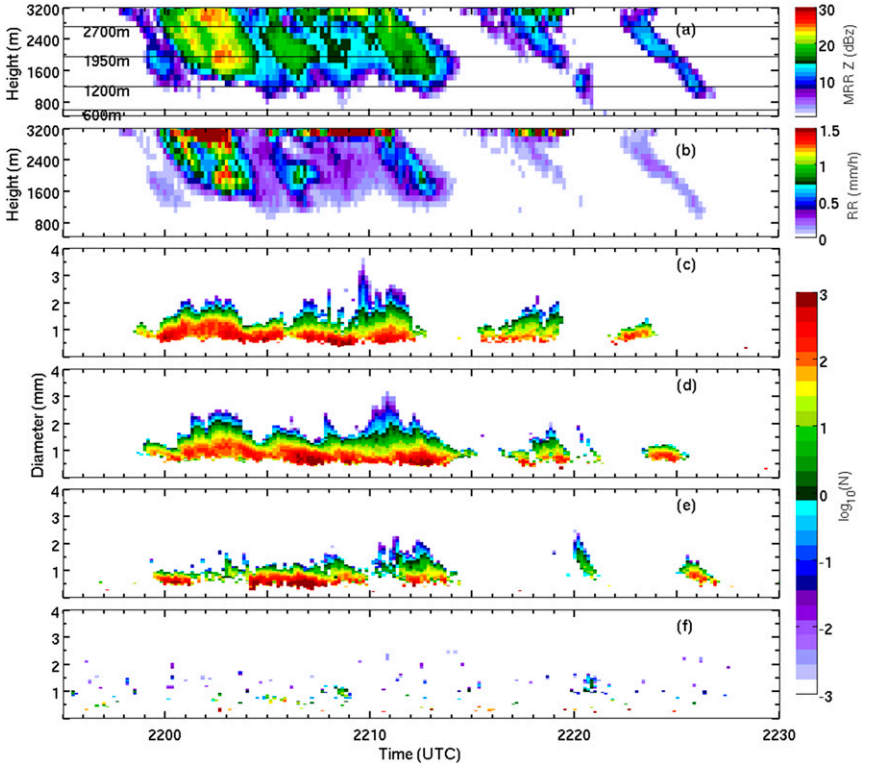


FIG. 8. As in Fig. 6, but between 2200 and 2230 UTC 4 Jul 2014.

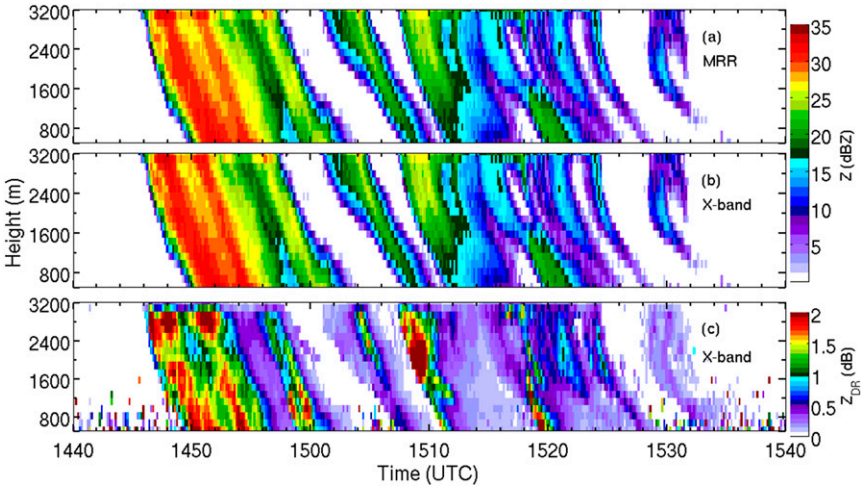


FIG. 9. (a) MRR-observed reflectivity. The terms (b) $Z$ and (c) $Z_{DR}$ simulated for X-band with the T-matrix method based on the vertical DSD profiles observed by the MRR between 1440 and 1540 UTC 4 Jul 2014.

$Z_{DR}$ aloft (Figs. 9 and 10), in agreement with Kumjian and Ryzhkov (2010), we can conclude that 1) low $Z_{DR}$ indicates the prevalence of smaller raindrops and leads to stronger evaporation and a decrease of $Z$ and rain rates toward the ground; and 2) a higher $Z_{DR}$ in the initial DSDs leads to a slower evaporation and a slow decrease of the rain rate toward the surface (1450–1500 UTC; Fig. 6). Before 1500 UTC (the first event), when $Z_{DR}$ is rather high aloft (larger raindrops), precipitation does not dissipate before reaching the ground. For the second event (between 2200 and 2230 UTC), the initially low $Z_{DR}$ (below 0.5 dB) indicates relatively small raindrops, leading to strong reductions in both reflectivity and rain rate toward the ground. Rain-rate reduction may approach 100% when the initial raindrops are sufficiently small and when the atmospheric conditions are sufficiently dry. Thus, for low rain rates with drizzlelike rainfall at the cloud base, it becomes essential to take evaporation into account.

To estimate the amount of the surface rainfall, we propose a retrieval algorithm that reduces the potential biases caused by evaporation. We relate $Z_{DR}$ aloft but below the melting layer to the surface rain rate based on the correlation between the initial $Z_{DR}$ and the surface rain-rate reduction found in the observations and simulations presented above. An example that describes in detail how the retrieval algorithm works is given in the following paragraph.

To validate this method and to quantify the surface rain rate using the MRR observations below the

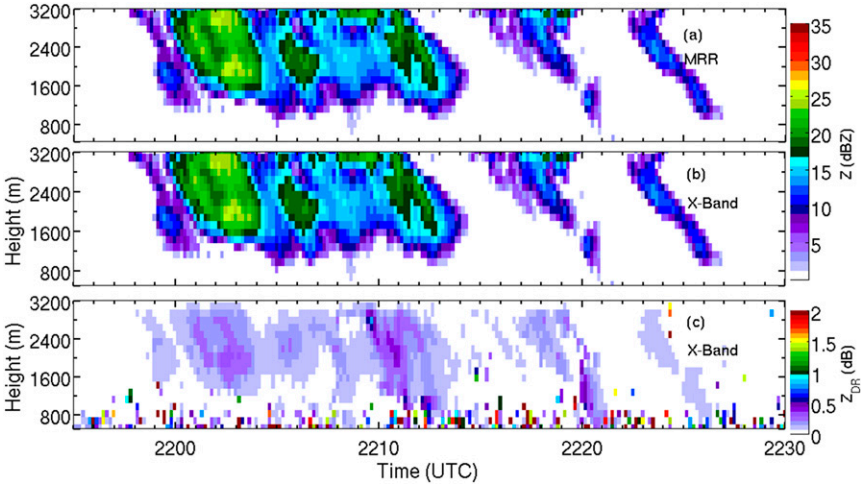


FIG. 10. As in Fig. 9, but for the period between 2155 and 2230 UTC 4 Jul 2014.

melting layer, we first apply the retrieval algorithm to MRR observations at subfreezing levels (the first event presented above). We take the MRR-observed DSD at 2100 m as "seeding" to avoid the effects of still melting particles and the dry layer observed by the radiosonde above 2300 m. With the evaporation model presented in section 2, $Z_{DR}$ and the related rain rates at all heights are calculated. Since the MRR is not observing the exact storm evolution, it is not possible to compare directly the MRR-observed surface rain rate with the simulated surface rain rate from DSD seeding aloft. Thus, here the robustness of the retrieval algorithm is achieved by comparing the simulated rain rates with the MRR-observed rain rates by their probability density functions (pdfs) for all levels between 600 and 1050 m between 1440 and 1540 UTC (Fig. 11).

Figure 12 shows for the same data the impact of the initial $Z_{DR}$ at 2100 m on the evaporation reduction of the rain rate at 600 m, using the algorithm presented above. Obviously, the initial $Z_{DR}$ aloft at 2100 m mainly determines the rain-rate reduction near the surface, which is only marginally affected by $Z$ aloft, given the atmospheric state below the melting layer. With $Z_{DR} < 0.5$ dB at 2100 m, the rain rate at 600 m can be reduced by more than 90%. For the initial $Z_{DR} >$ 2 dB, 20%–40% of the rainfall may be diminished by evaporation.

Our method can be extended for an estimation of surface rain using polarimetric radar measurements aloft in the presence of evaporation. It involves DSD retrievals at the lowest unobstructed elevations and application of the 1D evaporation model described in section 2. The initial DSD aloft at each radar pixel can be retrieved from the combination of $Z$ and $Z_{DR}$ using, for example, the algorithm described by Zhang et al. (2001). The required vertical profiles of temperature and humidity can be obtained from nearby radiosondes or from the output of numerical weather prediction (NWP) models.

The execution of DSD retrieval algorithm and 1D evaporation model at each pixel every 5–6 min in a whole precipitation area is possible with modern data processors. To further reduce computation time, we may use predetermined lookup tables for the ratio $\Delta R/R$ (rain-rate reduction/initial rain rate) as a function of $Z_{DR}$ aloft, depth of the evaporation layer, and vertical gradients and mean values of relative humidity and temperature as discussed by Kumjian and Ryzhkov (2010, their Fig. 11). They found that increases in $Z_{DR}$ aloft alleviate the rain-rate reduction on the ground, which is consistent with Fig. 12. However, Kumjian and Ryzhkov (their Fig. 11) predicted a rain-rate reduction by ~45% with the $Z_{DR}$ aloft of 2 dB and a surface relative humidity of 55%, while our Fig. 12 only indicates a rain-rate reduction of ~30%. As expected, using observed profiles leads to discrepancies with the idealized cases shown in Kumjian and Ryzhkov (2010), where 3-km-deep dry adiabatic layers with a surface temperature of 30°C were assumed. The observed case used in this study has a shallower lapse rate and cooler surface temperatures; thus, the lower rain-rate reduction in this study is not surprising.

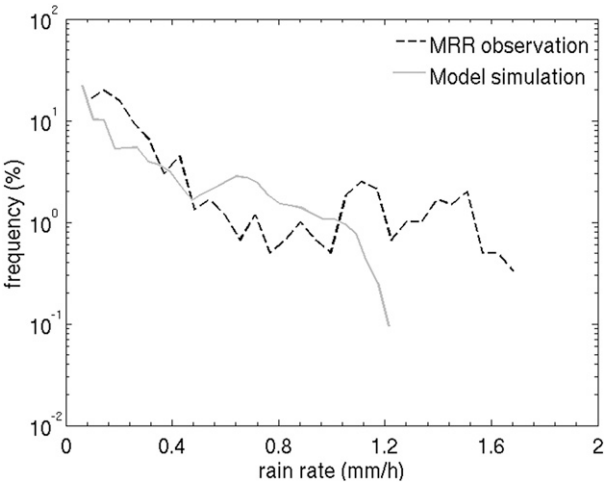


FIG. 11. The cumulative frequency distribution of model-simulated and MRR-observed RR between a height of 600 and 1050 m between 1440 and 1540 UTC 4 Jul 2014. The model-simulated RR is calculated with the evaporation model described in section 2, assuming the initial DSD observed by the MRR at 2100 m. The temperature profile is taken from the radiosonde launched at 1200 UTC in Essen.

## 5. Implications for cooling rate estimation

Evaporation of precipitation is considered as one of the most important processes contributing to cooling in the air (Dawson et al. 2010). It contributes to downdraft intensification and thus cold pool generation below precipitating clouds. Cold pools, which are regions of evaporatively cooled air under mature cumulus clouds, have been observed on many occasions (Zipser 1969; Houze 1977; Engerer et al. 2008). Cold pools play an important role in storm dynamics, particularly by interacting with the storm inflow as the less dense air is lifted above the cold pools, thus maintaining the updrafts and contributing to the development of new cells. This process is believed to be one of the main drivers of multicell thunderstorms.

Cooling rates caused by evaporation of rain are quantified by

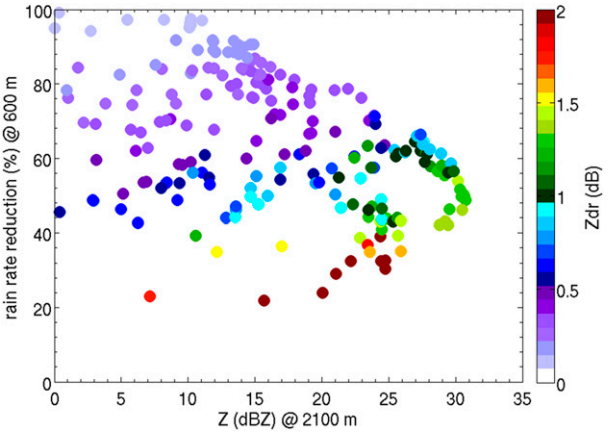


FIG. 12. Scatterplot between initial $Z$ at 2100 m and RR reduction at 600 m due to evaporation, with the color of the dots indicating the initial $Z_{DR}$ at 2100 m. The terms $Z$ and $Z_{DR}$ are the pseudo-observations of BoXPol at 2100 m between 1440 and 1540 UTC 4 Jul 2014 generated from the MRR-observed DSDs, while the RR difference between 2100 and 600 m is derived by the evaporation model described in section 2 using the initial DSDs at 2100 m from the MRR observations.

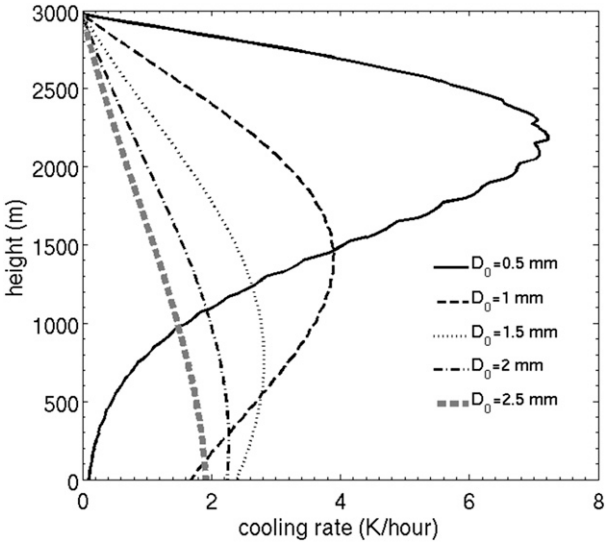


FIG. 13. Simulated vertical profiles of cooling rates as a function of height. The atmospheric conditions are described in section 2, assuming $\mu$ in the initial DSDs with a value of 2 and relative humidity on the ground of 50%.

$$\frac{\Delta T(z)}{\Delta t} = -\frac{L_v}{c_p \rho_a(z)} \int \frac{df(D,z)}{dz} m(D,0) N(D,z) [v_t(D,z) - w(z)] \, dD, \tag{7}$$

where $\Delta T(z)/\Delta t$ is the cooling rate, $L_v$ is the latent heat of vaporization, $c_p$ is the specific heat of dry air at constant pressure, $\rho_a$ is the air density, $m(D, 0)$ is the initial mass of a rain particle, $N(D, z)$ is the particle size distribution at height $z$, $v_t$ is the terminal velocity, $w$ is the vertical velocity of air, and $f$ is the fraction of mass left in the raindrop during evaporation. The function $f$, which contains the change of $D$ and $z$, can be derived by the rate of the change of the raindrop diameter described in section 2 and is used in the following calculations of cooling rates.

Figure 13 shows that the simulated cooling rate and its profile strongly depend on the initial DSDs. Smaller raindrops are more efficient producers of cooling and therefore of intense downdrafts (Srivastava 1985). Thus, small $D_0$ in DSDs leads to a high cooling rate peak of $7\,\mathrm{K\,h^{-1}}$ at 2000 m in our model setup, while rain with large $D_0$ evaporates more slowly but eventually results in cooling rates increasing toward the surface and reaching maxima of less than $3\,\mathrm{K\,h^{-1}}$. Note that the height of the peak of the cooling rate is related to $D_0$. For small $D_0$ the raindrops may totally evaporate before reaching the ground and thus maximum cooling rates are found aloft.

Taking the MRR-observed DSDs at 2100 m as initial values, we now apply Eq. (7) to the first event to calculate the resulting cooling rate profiles (Fig. 14). The cooling rate reaches up to $1.5\,\mathrm{K\,h^{-1}}$ at the beginning although the MRR-observed rain rate is only $\sim 2\,\mathrm{mm\,h^{-1}}$ between 1450 and 1500 UTC. After 1500 UTC, the estimated cooling rate stays below $0.4\,\mathrm{K\,h^{-1}}$ due to the even lower rain rate. The maximum of the estimated cooling rate is found above the surface, also for the second event, where smaller raindrops are prevalent (not shown), which is consistent with the sensitivity analysis presented in Fig. 13.

To estimate the evaporative cooling rates from the polarimetric radar observations, a similar procedure as described in section 4 can be used. The initial DSDs below the bottom of the melting layer are retrieved from $Z$ and $Z_{DR}$, and the atmospheric conditions are taken from NWP models or nearby radiosondes. Then the evaporative cooling rate at each height level can be obtained accordingly with the evaporation model. While this may be particularly useful in short-term weather forecasts, more extended validation efforts in the framework of a dedicated experiment with high-resolution radiosondes are required.

## 6. Conclusions and outlook

Together with simultaneous MRR observations, which allow for the estimation of vertical DSD profiles, polarimetric radar observations provide a quite detailed insight into DSD evolution and essential information for the estimation of the surface rain rate when evaporation is involved. We presented a sensitivity analysis of polarimetric

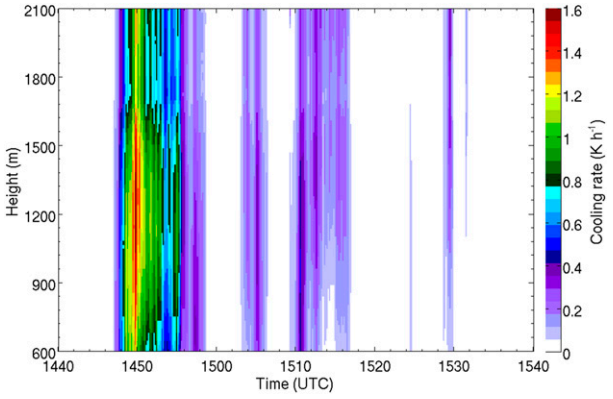


FIG. 14. Simulated cooling rate between the heights of 600 and 2100 m between 1440 and 1540 UTC 4 Jul 2014, assuming that the initial DSDs are observed by the MRR at 2100 m. The temperature profile is interpolated from the radiosonde launched at 1200 UTC in Essen.

variables to DSDs in the presence of raindrop evaporation for a range of atmospheric conditions. Both the X-band polarimetric radar and the K-band MRR observe the strong and exploitable connection between $Z_{DR}$ aloft and the surface rain-rate depletion by evaporation. We also investigated the cooling rates caused by evaporation and their dependence on the initial DSDs, which led us to propose an estimation algorithm for the surface rain rates and cooling rates based on $Z$ and $Z_{DR}$ observations aloft. The estimation algorithm for surface rain rates was validated with the MRR observations. The overall conclusions can be summarized as follows:

1) Raindrop evaporation leads to a decrease of $Z$ toward the surface, mostly accompanied with an increase of $Z_{DR}$ due to the predominant depletion of small raindrops and thus an increase of the DSD mean raindrop size, which is in agreement with previous studies (Li and Srivastava 2001; Kumjian and Ryzhkov 2010). A decrease of $Z_{DR}$ toward the surface can also be found, when the impact of the increasing temperature on the dielectric of water and thus the single-scattering properties of spheroid raindrops outweighs the effect of increasing mean raindrop size.
2) Our observations with an MRR and a polarimetric X-band radar showed that surface rain rates can be reduced significantly during evaporation. The observed reduction of surface rain rates increases with decreasing $Z_{DR}$ aloft, which is consistent with model simulations in previous studies (e.g., Kumjian and Ryzhkov 2010). Large raindrops (high $Z_{DR}$) evaporate more slowly than small raindrops (low $Z_{DR}$), and the complete evaporation of small raindrops may easily lead to complete rain-rate extinction near the surface.
3) Polarimetric radar observations can be used to estimate the evaporative cooling rate from the observed DSDs aloft and the evaporation model.
4) MRR observations can be used to develop and validate the retrieval method for rain rates near the ground using $Z$ and $Z_{DR}$ aloft observed by polarimetric radars. The method can be used for the estimation of surface rain rates at far distances from polarimetric radars and in case of beam blocking.

Considerable improvements of surface rain-rate estimates over complex terrain or at large distances from the radar can be made based on the observed $Z_{DR}$ aloft. A more comprehensive statistical analysis for a range of climatic conditions is, however, needed to devise a generally applicable algorithm and to extend it to other radar bands. Future studies should focus on the quantification of evaporation with combined observations of polarimetric radars and surface rainfall over a wide range of the atmospheric conditions, and comparisons with simulations.

During the analyzed event, advection was taking place between the signatures just below the bright band and where the rain is falling to the surface, which makes retrievals challenging. We thus recommend the use of this method with radar observations available at lower levels which are significantly above the ground instead of just below the bright band, in order to reduce the errors caused by additional microphysical processes influencing the polarimetric moments.

So far, only evaporation has been taken into account in our 1D model. Thus, the proposed applications are limited to light and moderate rain, when other processes acting on DSDs are less relevant. Size sorting, coalescence, and breakup also change the DSDs during fall and may result in significant uncertainties in the relations derived especially in heavy rainfall.

*Acknowledgments.* This work has been funded by the Federal Ministry of Education and Research in Germany (BMBF) through the research program "High Definition Clouds and Precipitation for Climate Prediction" [HD(CP)$^2$] (FKZ: 01LK1219A and 01LK1210A). Funding for A. Ryzhkov was provided by NOAA/Office of Oceanic and Atmospheric Research under NOAA–University of Oklahoma Cooperative Agreement NA11OAR4320072, U.S. Department of Commerce. We thank Martin Lennefer and Kai Muehlbauer at the University of Bonn and the SFB/TR 32 (Transregional Collaborative Research Centre 32; http://www.tr32.de/), funded by the German Research Foundation (DFG), for maintaining the instruments and for making the BoXPol and MRR data available. We thank

the editor and two anonymous reviewers for their valuable comments, which helped us to greatly improve the paper.

## REFERENCES


Anagnostou, M. N., E. N. Anagnostou, J. Vivekanandan, and F. L. Ogden, 2008: Comparison of two raindrop size distribution retrieval algorithms for X-band dual polarization observations. *J. Hydrometeor.*, **9**, 589–600, doi:10.1175/2007JHM904.1.

Borowska, L., D. Zrnić, A. Ryzhkov, P. Zhang, and C. Simmer, 2011: Polarimetric estimates of a 1-month accumulation of light rain with a 3-cm wavelength radar. *J. Hydrometeor.*, **12**, 1024–1039, doi:10.1175/2011JHM1339.1.

Brandes, E. A., G. Zhang, and J. Vivekanandan, 2002: Experiments in rainfall estimation with a polarimetric radar in a subtropical environment. *J. Appl. Meteor.*, **41**, 674–685, doi:10.1175/1520-0450(2002)041<0674:EIREWA>2.0.CO;2; Corrigendum, **44**, 186, doi:10.1175/1520-0450(2005)44<186:C>2.0.CO;2.

——, ——, and ——, 2004: Drop size distribution retrieval with polarimetric radar: Model and application. *J. Appl. Meteor.*, **43**, 461–475, doi:10.1175/1520-0450(2004)043<0461:DSDRWP>2.0.CO;2.

Bringi, V., and V. Chandrasekar, 2001: *Polarimetric Doppler Weather Radar: Principles and Applications.* Cambridge University Press, 636 pp.

Cao, Q., and Y. Qi, 2014: The variability of vertical structure of precipitation in Huaihe River Basin of China: Implications from long-term spaceborne observations with TRMM precipitation radar. *Water Resour. Res.*, **50**, 3690–3705, doi:10.1002/2013WR014555.

Comstock, K. K., R. Wood, S. E. Yuter, and C. S. Bretherton, 2004: Reflectivity and rain rate in and below drizzling stratocumulus. *Quart. J. Roy. Meteor. Soc.*, **130**, 2891–2918, doi:10.1256/qj.03.187.

Dawson, D. T., M. Xue, J. A. Milbrandt, and M. K. Yau, 2010: Comparison of evaporation and cold pool development between single-moment and multimoment bulk microphysics schemes in idealized simulations of tornadic thunderstorms. *Mon. Wea. Rev.*, **138**, 1152–1171, doi:10.1175/2009MWR2956.1.

Diederich, M., A. Ryzhkov, C. Simmer, P. Zhang, and S. Trömel, 2015: Use of specific attenuation for rainfall measurement at X-band radar wavelengths. Part I: Radar calibration and partial beam blockage estimation. *J. Hydrometeor.*, **16**, 487–502, doi:10.1175/JHM-D-14-0066.1.

Engerer, N. A., D. J. Stensrud, and M. C. Coniglio, 2008: Surface characteristics of observed cold pools. *Mon. Wea. Rev.*, **136**, 4839–4849, doi:10.1175/2008MWR2528.1.

Gorgucci, E., V. Chandrasekar, and L. Baldini, 2008: Microphysical retrievals from dual-polarization radar measurements at X band. *J. Atmos. Oceanic Technol.*, **25**, 729–741, doi:10.1175/2007JTECHA971.1.

Gori, E. G., and J. Joss, 1980: Changes of shape of raindrop size distributions simultaneously observed along a mountain slope. *J. Rech. Atmos.*, **14**, 239–300.

Houze, R. A. J., 1977: Structure and dynamics of a tropical squall-line system. *Mon. Wea. Rev.*, **105**, 1540–1567, doi:10.1175/1520-0493(1977)105<1540:SADOAT>2.0.CO;2.

Hu, Z., and R. C. Srivastava, 1995: Evolution of raindrop size distribution by coalescence, breakup, and evaporation: Theory and observations. *J. Atmos. Sci.*, **52**, 1761–1783, doi:10.1175/1520-0469(1995)052<1761:EORSDB>2.0.CO;2.

Kim, D. S., M. Maki, and D. I. Lee, 2010: Retrieval of three-dimensional raindrop size distribution using X-band polarimetric radar data. *J. Atmos. Oceanic Technol.*, **27**, 1265–1285, doi:10.1175/2010JTECHA1407.1.

Kneifel, S., M. Maahn, G. Peters, and C. Simmer, 2011: Observation of snowfall with a low-power FM-CW K-band radar (Micro Rain Radar). *Meteor. Atmos. Phys.*, **113**, 75–87, doi:10.1007/s00703-011-0142-z.

Kumjian, M. R., and A. V. Ryzhkov, 2010: The impact of evaporation on polarimetric characteristics of rain: Theoretical model and practical implications. *J. Appl. Meteor. Climatol.*, **49**, 1247–1267, doi:10.1175/2010JAMC2243.1.

——, and O. P. Prat, 2014: The impact of raindrop collisional processes on the polarimetric radar variables. *J. Atmos. Sci.*, **71**, 3052–3067, doi:10.1175/JAS-D-13-0357.1.

Li, X., and R. C. Srivastava, 2001: An analytical solution for raindrop evaporation and its application to radar rainfall measurements. *J. Appl. Meteor.*, **40**, 1607–1616, doi:10.1175/1520-0450(2001)040<1607:AASFRE>2.0.CO;2.

Mishchenko, M. I., 2000: Calculation of the amplitude matrix for a nonspherical particle in a fixed orientation. *Appl. Opt.*, **39**, 1026–1031, doi:10.1364/AO.39.001026.

Penide, G., V. V. Kumar, A. Protat, and P. T. May, 2013: Statistics of drop size distribution parameters and rain rates for stratiform and convective precipitation during the north Australian wet season. *Mon. Wea. Rev.*, **141**, 3222–3237, doi:10.1175/MWR-D-12-00262.1.

Prat, O. P., and A. P. Barros, 2007: A robust numerical solution of the stochastic collection–breakup equation for warm rain. *J. Appl. Meteor. Climatol.*, **46**, 1480–1497, doi:10.1175/JAM2544.1.

Pruppacher, H. R., and J. D. Klett, 1997: *Microphysics of Clouds and Precipitation.* Kluwer Academics, 594 pp.

Rasmussen, R. M., and A. J. Heymsfield, 1987: Melting and shedding of graupel and hail. Part I: Model physics. *J. Atmos. Sci.*, **44**, 2754–2763, doi:10.1175/1520-0469(1987)044<2754:MASOGA>2.0.CO;2.

Rogers, R. R., and M. K. Yau, 1989: *A Short Course in Cloud Physics.* 3rd ed. Elsevier Press, 290 pp.

Rosenfeld, D., and Y. Mintz, 1988: Evaporation of rain falling from convective clouds as derived from radar measurements. *J. Appl. Meteor.*, **27**, 209–215, doi:10.1175/1520-0450(1988)027<0209:EORFFC>2.0.CO;2.

Ryzhkov, A. V., S. E. Giangrande, V. M. Melnikov, and T. J. Schuur, 2005: Calibration issues of dual-polarization radar measurements. *J. Atmos. Oceanic Technol.*, **22**, 1138–1155, doi:10.1175/JTECH1772.1.

Saavedra, P., A. Battaglia, and C. Simmer, 2012: Partitioning of cloud water and rainwater content by ground-based observations with the Advanced Microwave Radiometer for Rain Identification (ADMIRARI) in synergy with a micro rain radar. *J. Geophys. Res.*, **117**, D05203, doi:10.1029/2011JD016579.

Seifert, A., 2008: On the parameterization of evaporation of raindrops as simulated by a one-dimensional rainshaft model. *J. Atmos. Sci.*, **65**, 3608–3619, doi:10.1175/2008JAS2586.1.

Srivastava, R. C., 1985: A simple model of evaporatively driven downdraft: Application to microburst downdraft. *J. Atmos. Sci.*, **42**, 1004–1023, doi:10.1175/1520-0469(1985)042<1004:ASMOED>2.0.CO;2.

——, 1987: A model of intense downdrafts driven by the melting and evaporation of precipitation. *J. Atmos. Sci.*, **44**, 1752–1774, doi:10.1175/1520-0469(1987)044<1752:AMOIDD>2.0.CO;2.

Testud, J., S. Oury, R. A. Black, P. Amayenc, and X. Dou, 2001: The concept of ''normalized'' distribution to describe raindrop spectra: A tool for cloud physics and cloud remote sensing. *J. Appl. Meteor.*, **40**, 1118–1140, doi:10.1175/1520-0450(2001)040<1118:TCONDT>2.0.CO;2.

Willis, P. T., 1984: Functional fits to some observed drop size distributions and parameterization of rain. *J. Atmos. Sci.*, **41**, 1648–1661, doi:10.1175/1520-0469(1984)041<1648:FFTSOD>2.0.CO;2.

Zhang, G., J. Vivekanandan, and E. Brandes, 2001: A method for estimating rain rate and drop size distribution from polarimetric radar measurements. *IEEE Trans. Geosci. Remote Sens.*, **39**, 830–841, doi:10.1109/36.917906.

Zipser, E. J., 1969: The role of organized unsaturated convective downdrafts in the structure and rapid decay of an equatorial disturbance. *J. Appl. Meteor.*, **8**, 799–814, doi:10.1175/1520-0450(1969)008<0799:TROOUC>2.0.CO;2.